Multimodal map and complex basin of attraction of a simple hopper

C. K. Reddy
Department of Engineering Science and Mechanics, Virginia Polytechnic Institute and State University, Blacksburg, Virginia 24061, USA

R. Pratap*
Department of Mechanical Engineering, Indian Institute of Science, Bangalore-560012, India

(Received 11 August 2002; revised manuscript received 23 December 2002; published 24 July 2003)

In this paper, we study the global dynamics of a simple passive mechanical model for hopping. The hopper is a two-mass, single-spring system constrained to move in the vertical direction (under gravity) above a rigid ground. The hopper model and its basic dynamics including the existence of incessant hopping motions have been reported elsewhere. Here, we extend the study to investigate the global dynamics of the hopper. The global map of the hopper is multimodal. We construct an approximate analytic map near the fixed points of the map and show that the fixed points exhibit one-way stability. We also show that the map is invariant under the inversion of the mass ratio of the hopper. Next, we construct the global basin of attraction of these fixed points and show that their structure is highly complex and retains form at finer scales. This structure of the basin of attraction contains regions where the fate of an arbitrary initial condition becomes unpredictable.

DOI: 10.1103/PhysRevE.68.016220 PACS number(s): 05.45.−a, 05.10.−a, 82.40.Bj

I. INTRODUCTION

We consider the passive hopper model studied by Chatterjee *et al.* [1]. The model consists of two masses m_1 and m_2 connected together with a spring and is allowed to move only vertically under gravity above a rigid ground (see Fig. 1). The collisions of the lower mass with the ground are assumed to be perfectly plastic. The motivation behind this model is to study the energetics of such a locomotion without overwhelming it with external controls. Passive systems provide much insight into natural dynamics and a better starting point for controls as advocated by the works of McGeer [2] and subsequent researchers [3,4]. Chatterjee *et al.* have studied the basic dynamics and associated properties of the passive hopper. The most interesting and relevant result of their investigation is the existence of energy conserving periodic motions of the hopper, termed *incessant hopping* in Ref. [1]. They also show the existence of a similar motion in a juggling model and establish an equivalence between the two models. Schiehlen and Gao [5], however, were the first to discover lossless motions of this model but their investigations were cursory. Approximately simultaneously with Chatterjee *et al.*, and independently, Hagerty [6] investigated the existence of such a motion in the context of a bouncing eccentric cylinder and reached similar conclusions. Our work here is based on the more-available and directly applicable [1].

The mechanical model, shown in Fig. 1, is simple; the motions it exhibits, as we show later, are complex. That, a simple deterministic dynamical system exhibits complex behavior [7], is not surprising anymore. Yet, the dynamics we investigate here is remarkable because of its existence in several simple mechanical systems such as hoppers, jugglers [1], and galloping models [6,8]. These models are capable of persistent energy conserving motions in an overwhelmingly dissipative phase space. These motions exhibit one-way stability, a fact usually dismissed as a pathological case in mathematical theories of dynamical systems [9]. However, one-way stable limit cycles are known to exist in bilinear models of elastoplastic oscillators [10].

If we let our mechanical intuition guide us in imagining the varied motions that this hopper can have, the plastic collision of the lower mass with the ground is likely to mess up our intuition for motions beyond the simple ones (such as the lower mass stopping dead with a thud on the ground while the upper mass oscillates). The collisions play an equally destructive role mathematically by destroying the otherwise smooth flow of the underlying dynamical system. The collisions introduce jumps in the state of the system, providing nonlinearity that is perhaps best modeled as discrete events. This mixing of continuous flow and discrete events makes it a hybrid dynamical system. Although, the literature on hybrid dynamical systems is fairly rich, much of it is motivated by mixed control strategies (see, for example, Ref. [11] and references therein). Here, we are interested in the discrete events (impacts with the ground) mainly as the instants of instantaneous change in the state of the system. Several systems with intermittent contacts [12,13] form examples of such dynamical systems.

The simplicity of the model and the nonsmoothness intro-

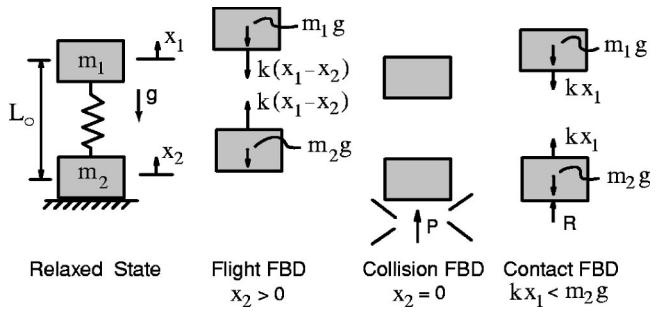

FIG. 1. The figure shows the passive hopper and the different phases during its motion (taken from Ref. [1]).

*Electronic address: pratap@mecheng.iisc.ernet.in

duced by the collisions make *maps* an ideal choice for studying the dynamics of this system. However, we cannot obtain explicit maps as discussed in Ref. [1]. Chatterjee *et al.* constructed the map numerically and studied its properties geometrically. The map turns out to be multimodal, i.e., it has many humps. Here, we construct an approximate analytical map near the fixed points (that correspond to the incessant hopping motions) and show that the fixed points are one-way stable as stated in Ref. [1] based on geometric properties of the numerical map. In addition, we show that the approximate map is invariant under the mass reciprocity of the hopper which implies that the dynamics near the fixed points is unaffected if the upper and the lower masses are interchanged. We then proceed to construct the basin of attraction of the incessant motions and show that it has a complex structure. The complexity of the structure is evident from the numerically generated basins of attractions that retain structure at finer scales. We also compute numerically the measure of this basin for two selected values of the mass ratio and show that the measure is very sensitive to the mass ratio.

II. EQUATIONS OF MOTION AND LOSSLESS SOLUTIONS

The equations of motion of the system, the conditions for lossless solutions, and the general nature of solutions are described in detail in Ref. [1]. In this section, we reproduce, in brief, the equations of motion and some of the associated dynamics from Ref. [1] so that the reader can follow the main discussion of the paper from Sec. III with relative ease.

The equations of motion of the system can be written with the help of the free body diagrams shown in Fig. 1. The system behavior is best represented by separate equations for in-flight dynamics, collision transition, and dynamics during sustained contact of the lower mass with the ground. We use the following nondimensional variables for the equations of motion:

$$y_1 \equiv \frac{x_1}{(m_2 g/k)}, \quad y_2 \equiv \frac{x_2}{(m_2 g/k)}, \quad M \equiv \frac{m_2}{m_1}, \quad (\dot{}) \equiv \frac{d(\ )}{d\tau},$$

where $\tau = \omega t$ and $\omega = \sqrt{k(1+M)/m_2}$ is the angular frequency of vibration in the flight phase.

(*a*). *Flight.* The equations of motion for free flight in terms of the new variables are (see Fig. 1)

$$(1+M)\ddot{y}_1 = -M(y_1 - y_2) - 1,$$

$$(1+M)\ddot{y}_2 = (y_1 - y_2) - 1. \tag{1}$$

(*b*). *Collision transition.* When the lower mass lands on the ground, the collision causes a jump in its velocity but not in its displacement. Using ''$-/+$'' to denote before and after impact, the collision occurs when $y_2^- = 0$ and $\dot{y}_2^- \leqslant 0$. The impact transitions are $y_1^+ = y_1^-$; $y_2^+ = y_2^- = 0$; $\dot{y}_1^+ = \dot{y}_1^-$; and $\dot{y}_2^+ = 0$.

(*c*). *Contact.* During a period of sustained contact, $y_2 \equiv 0$, $y_1 < 1$, and $(1+M)\ddot{y}_1 = -My_1 - 1$.

(*d*). *Lift-off transition.* Lift-off from the ground contact occurs when the spring tension lifts the lower mass and $y_1 = 1$. The lift-off condition can also be met immediately at contact with no period of sustained contact (if $y_1^- > 1$). At lift-off from sustained contact there is no jump in position or velocity of either mass.

We define $\alpha \equiv \dot{y}_1$ at lift-off after a period of sustained contact. α is the key variable in the following analysis. The positions and velocities at the instant of lift off are

$$y_1 = 1; \ \dot{y}_1 = \alpha; \ y_2 = 0; \ \dot{y}_2 = 0. \tag{2}$$

These serve as initial conditions for the flight equations. Note that all subsequent motions for all time are determined by α at one lift-off. Thus, the dynamics can be characterized by a one-dimensional (1D) map, $\alpha_{n+1} = f(\alpha_n)$ as seen in Sec. III.

Lossless solutions

An impact with nonzero speed would be dissipative. Thus, for no dissipation, $\dot{y}_2 = 0$ at $y_2 = 0$. For sustained lossless motions, we also need conditions on the acceleration and jerk apart from the zero speed condition. If $\ddot{y}_2 > 0$, contact would be immediately lost and there would be a subsequent collision with nonzero speed, and $\ddot{y}_2 < 0$ would require prior ground penetration which is not possible physically. Thus, for lossless impact at $y_2 = 0$, not only $\dot{y}_2 = 0$ but also $\ddot{y}_2 = 0$. Because $\ddot{y}_2 = 0$, the ground clearance condition is determined by $d^3 y_2/d\tau^3$. If $d^3 y_2/d\tau^3 > 0$, grazing would be followed by a dissipative impact and hence there will be no subsequent sustained lossless motions. Thus, we must simultaneously meet all of these conditions at the end of flight:

$$y_2 = 0, \ \dot{y}_2 = 0, \ \ddot{y}_2 = 0, \ \text{and} \ \ d^3 y_2/d\tau^3 < 0.$$

All of these conditions can be simultaneously met in this model, no matter what the values of the model parameters, by adjustment of the single dynamic variable α (the lift-off speed of m_1). To find these lossless solutions, we first solve the initial value problem for the flight phase [Eqs. (1) and (2)]. Imposing the dissipation-free contact conditions on the solution at the end of the flight, we can solve for the time of flight in terms of α. Then substituting this relationship in the zero acceleration condition for sustained contact, we finally get (see Ref. [1] for details)

$$\alpha = \tan \alpha. \tag{3}$$

Equation (3) has infinitely many solutions for α (and hence for τ_f). These solutions for α which give incessant hopping are denoted by α^* and $= 4.493\,409$, $7.725\,251$, $10.904\,12, \ldots$. Higher values of α^* correspond to more oscillations between collisions.

III. ONE-DIMENSIONAL MAP AND THE GENERAL DYNAMICS OF THE HOPPER

The dynamics of the hopper between two gradual lift-offs can be studied by constructing a map of the form

$$\mathbf{Y}_{n+1}=F(\mathbf{Y}_n), \tag{4}$$

where $\mathbf{Y}=[y_1\ \dot{y}_1]^T$ is the state vector of the upper mass and $F:\mathbf{R}^2\mapsto\mathbf{R}^2$ maps $\mathbf{Y}$ from the n^{th} gradual lift-off to the $(n+1)^{th}$ gradual lift-off. F is defined as

$$F\equiv F_c\circ F_f\circ F_f\circ\cdots\circ F_f, \tag{5}$$

where F_f is the flight-impact map and F_c is the contact map. Note that there can be more than one flight-impact maps and these correspond to immediate lift-offs without any period of steady contact. F_f and F_c are defined as

$$F_f(\mathbf{Y})=\left\{\begin{array}{c}\dfrac{y_1+\dot{y}_1\tau_f-\dfrac{\tau_f^2}{2}+M(\dot{y}_1\sin\tau_f+y_1\cos\tau_f)}{1+M}\\ \dfrac{\dot{y}_1-\tau_f+M(\dot{y}_1\cos\tau_f-y_1\sin\tau_f)}{1+M}\end{array}\right\}, \tag{6}$$

$$F_c(\mathbf{Y})=\left\{\begin{array}{c}1\\ \sqrt{\dfrac{(1+M)\dot{y}_1^2+M\,y_1^2+2y_1-2-M}{1+M}}\end{array}\right\}, \tag{7}$$

where the time of flight τ_f satisfies

$$\frac{\tau_f^2}{2}+\dot{y}_1\sin\tau_f+y_1\cos\tau_f-\dot{y}_1\tau_f-y_1=0. \tag{8}$$

Since

$$\mathbf{Y}_n=\left\{\begin{array}{c}1\\ \alpha_n\end{array}\right\},$$

Eq. (4) is essentially a one-dimensional map of the form

$$\alpha_{n+1}=f(\alpha_n). \tag{9}$$

The map $f:R\mapsto R$ cannot be written explicitly since the solution of the flight equations involves transcendental functions. Therefore, we construct the map numerically. A few maps corresponding to some typical values of the mass ratio M are shown in Fig. 2 where the multimodality of the map is self evident. The fixed points of this map correspond to the solutions of $\alpha=\tan\alpha$. We have plotted the map only up to the first five fixed points but the trend is clear enough not to warrant a longer map for our studies. The map by itself does not give enough information about the physical motion of the hopper with different initial conditions. We can, however, use the map to characterize the physical motion by considering the set of initial conditions around a single fixed point and the unimodal map around it (a single hump). We could, for example, divide the region around the first nontrivial

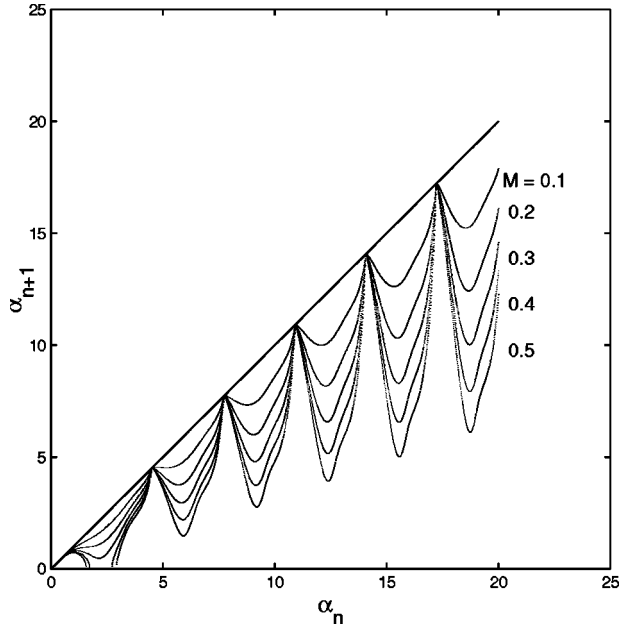

FIG. 2. The one-dimensional map on the free variable α, the nondimensional velocity of the upper mass, tracked between two successive gradual hops. Different maps correspond to different values of the mass ratio M.

fixed point $\alpha^{*1}=4.4934$ into four segments—α_L, α_B, α_R, and α_G—as shown in Fig. 3 and show a typical motion of the hopper in each segment. In α_L, the landing of the lower mass is followed by an immediate takeoff at the expense of huge loss of energy in the impact, which makes subsequent takeoffs to be increasingly difficult. The fixed point exhibits one-way stability (We prove the stability of the fixed point in Sec. IV.) We denote the local interval of attraction as α_B. In α_B, the dynamics eventually settles down to energy conserving periodic hops. Since this incessant motion is very special, we discuss it in the following sections. On the right segment of the hump, a typical motion of the hopper in α_R involves one or two gradual hops of the lower mass before it settles down to the ground, while the upper mass continues to oscillate (as a single degree of freedom, undamped oscillator). The open segment of the map, α_G, represents motions that have no hops at all. The motions described above are just representative motions. It turns out that α_L and α_R are not continuous segments. They have rather complicated structure which we describe in Sec. VI. It is worth mentioning here that the nonsmooth transition of the map from α_L to α_B (from a linear segment to a parabolic segment) is reflective of the qualitatively different motions of the hopper in the two segments. On the right side of the fixed point α^*, we have $y_1^-<1$ at impact. This condition implies that for all initial velocities of the form $\alpha_n=\alpha^*+\delta\alpha$, there is no sudden takeoff. However, on the other hand, for initial conditions to the left of the fixed point, i. e., conditions of the form $\alpha_n=\alpha^*-\delta\alpha$, we have $y_1^->1$. This condition assures that the spring has enough force to pull the lower mass immediately after impact (sudden takeoff), which is then followed by a second impact and further loss of energy. This motion leads to a further decrease in the value of α_{n+1}. The one-dimensional

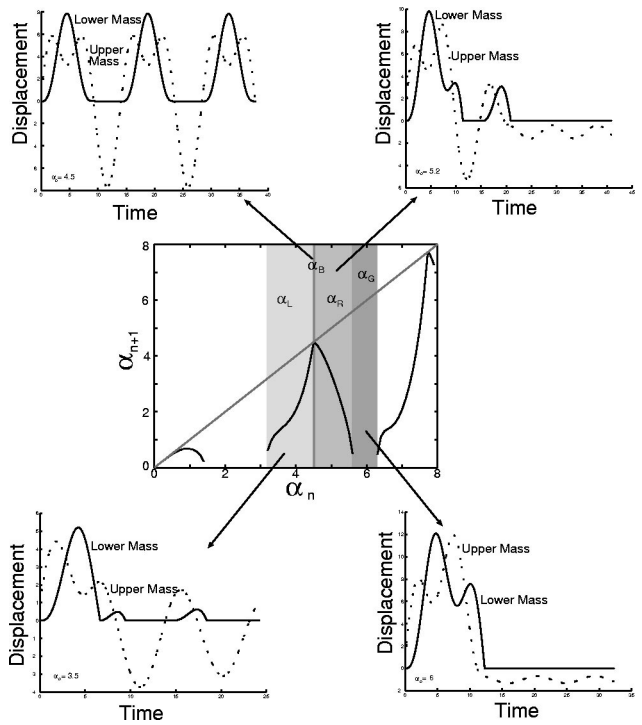

FIG. 3. Typical dynamics of the hopper on various segments of the map. The region around a fixed point is divided into four segments: α_L represents the left leg of the map, α_B represents the local basin of attraction of the fixed point, α_R represents the right leg of the map, and α_G represents the gap between two map segments. Typical motions of the hopper in each segment are shown in the adjacent plots.

map, therefore, curves downwards on the left side of the fixed point. The general nature of the motions of the hopper described above is repeated in similar segments of the other humps of the map, with one basic but inconsequential difference that the mid-air oscillations increase in all segments as we consider humps associated with higher fixed points.

IV. STABILITY OF THE LOSSLESS MOTIONS

The fixed points of the 1D map correspond to energy conserving motions of the hopper. We carry out a higher-order perturbation of the map around any fixed point α^* in order to determine the stability of the fixed point and estimate the interval of attraction, if stable. An interval of attraction on the left, close to the fixed point, would require the one-dimensional map to lie above the line of unit slope, which is not admissible from energy considerations. In what follows, we show that the fixed point has a nonzero interval of attraction on the right side. Consider the initial conditions at the n^{th} gradual hop,

$$\mathbf{Y}_n = \begin{Bmatrix} 1 \\ \alpha_n \end{Bmatrix}.$$

The time of flight then satisfies

$$\frac{\tau_f^2}{2} + \alpha_n \sin\tau_f + \cos\tau_f - \alpha_n \tau_f - 1 = 0, \tag{10}$$

where $\alpha_n = \alpha^* + \delta\alpha$ with $\delta\alpha \ll 1$. Equation (10) is rearranged as

$$\alpha_n = \frac{\frac{\tau_f^2}{2} + \cos\tau_f - 1}{\tau_f - \sin\tau_f} = \phi(\tau_f). \tag{11}$$

A Taylor series expansion around τ^* (time of flight corresponding to α^*) yields

$$\delta\alpha = \frac{\partial\phi}{\partial\tau_f}\delta\tau_f + \frac{1}{2}\frac{\partial^2\phi}{\partial\tau_f^2}(\delta\tau_f)^2 + \frac{1}{6}\frac{\partial^3\phi}{\partial\tau_f^3}(\delta\tau_f)^3 + \cdots. \tag{12}$$

The fixed point α^* satisfies

$$\alpha^*\sin(2\alpha^*) + \cos(2\alpha^*) = 1,$$

$$\alpha^*\cos(2\alpha^*) - \sin(2\alpha^*) = -\alpha^*. \tag{13}$$

Using Eqs. (10) and (13), it can be shown that

$$\frac{\partial\phi}{\partial\tau_f}(\tau^*) = \frac{\partial^2\phi}{\partial\tau_f^2}(\tau^*) = 0; \quad \frac{\partial^3\phi}{\partial\tau_f^3}(\tau^*) = \frac{\alpha^*}{2\alpha^* - \sin(2\alpha^*)}.$$

Neglecting the higher-order terms in $\delta\tau$, we have

$$\delta\tau = \beta(\delta\alpha)^{1/3}, \tag{14}$$

where

$$\beta = \left[\frac{6[2\alpha^* - \sin(2\alpha^*)]}{\alpha^*}\right]^{1/3}.$$

In Sec. III, we noted that for initial conditions of the form $\alpha_n = \alpha^* + \delta\alpha$, we have a period of sustained contact at landing. Equation (4), thus, is

$$\mathbf{Y}_{n+1} = F(\mathbf{Y}_n) = F_c \circ F_f(\mathbf{Y}_n).$$

Equations (6) and (7) give

$$\alpha_{n+1} = \sqrt{\frac{(1+M)(\dot{y}_1)^2 + M(y_1)^2 + 2y_1 - 2 - M}{1+M}}, \tag{15}$$

where

$$y_1 = \frac{M(\alpha_n \sin\tau_f + \cos\tau_f) + \alpha_n\tau_f + 1 - (\tau_f^2/2)}{1+M},$$

$$\dot{y}_1 = \frac{\alpha_n + M(\alpha_n\cos\tau_f - \sin\tau_f) - \tau_f}{1+M}. \tag{16}$$

Note that when $\alpha_n = \alpha^*$,

$$F_f(\mathbf{Y}_n)=\begin{Bmatrix} 1 \\ -\alpha^* \end{Bmatrix}.$$

A variation $\delta\alpha_1$ in α_{n+1} can be written as

$$\delta\alpha_1=\frac{\delta y_1}{\alpha^*}-\delta\dot{y}_1+\frac{M}{2\alpha^*(1+M)}(\delta y_1)^2+\frac{1}{2\alpha^*}(\delta\dot{y}_1)^2+\cdots, \tag{17}$$

where δy_1 and $\delta\dot{y}_1$ are the variations in y_1 and $\dot{y}_1$, respectively. Using Eqs. (14) and (16) in (17), and neglecting the higher-order terms, we get

$$\delta\alpha_1\approx\delta\alpha-\frac{\beta M[2\alpha^*-\sin(2\alpha^*)]}{(1+M)^2}(\delta\alpha)^{4/3}. \tag{18}$$

Thus, the one-dimensional map close to the fixed point α^* is given as

$$\alpha_{n+1}=\alpha_n-\lambda(\alpha_n-\alpha^*)^{4/3}, \tag{19}$$

where $\lambda=\beta M[2\alpha^*-\sin(2\alpha^*)]/(1+M)^2$. It is clear that α^* is a fixed point and that the linearized map has a multiplier equal to 1. This condition would not guarantee stability for a general 1D map. However, in our physical system, energy dissipation prevents the map from lying above the line of unit slope. This clearly proves that the fixed point exhibits one-way stability.

A. Estimate of the local basin of attraction

The size Δ of the interval of attraction can be estimated by setting $\delta\alpha_1=0$ and $\delta\alpha=\Delta$ in Eq. (18). The interval of attraction is approximately given as

$$\Delta=\frac{1}{\lambda^3}. \tag{20}$$

Now, λ has a maximum value at $M=1$. Therefore, we expect the size of the interval of attraction to be minimum at $M=1$. In the following section, we show that this is also the case for the exact map. Specifically, we show that the map is invariant when M is replaced by $1/M$. Equation (19) clearly shows the invariance for the approximate map. Figure 4 compares the approximate map and the exact map (numerical) for $M=1$.

B. Invariance of the one-dimensional map

The mass ratio M is the only system parameter in the map. A study of the map variation with M is important for understanding the underlying dynamics. We prove the following results for the 1D map.

Result. The one-dimensional map $\alpha_{n+1}=f(\alpha_n,M)$ is invariant under $M\rightarrow 1/M$ when there is no sudden jump between two successive iterates of the map.

Mathematically, the above result is expressed as

$$\alpha_{n+1}=f(\alpha_n,M)=f(\alpha_n,1/M).$$

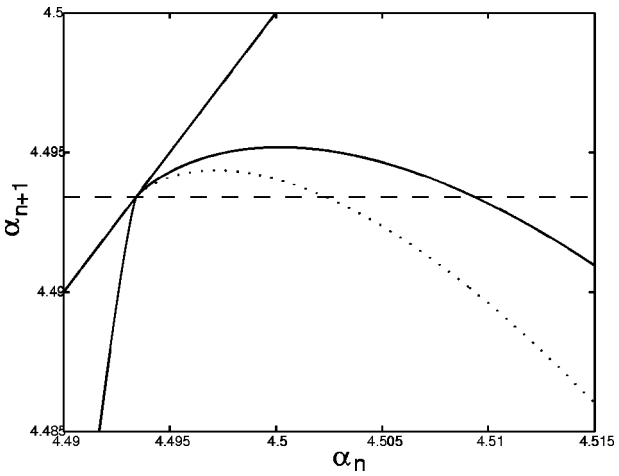

FIG. 4. Comparison between the exact numerical map (solid line) and the approximate map (dotted line).

Using Eq. (10), Eq. (16) is written as

$$\begin{aligned} y_1&=\alpha_n\sin\tau_f+\cos\tau_f \\ &=a \quad \text{(say)}, \\ \dot{y}_1&=\frac{\alpha_n-\tau_f+M(\alpha_n\cos\tau_f-\sin\tau_f)}{1+M} \\ &=\frac{a_1+M\,b_1}{1+M}. \end{aligned} \tag{21}$$

Equation (15), thus, becomes

$$\alpha_{n+1}=\sqrt{\frac{(1+M^2)\alpha_n^2}{(1+M)^2}+\frac{M[a^2+2(a-1)+2a_1b_1-1]}{(1+M)^2}}, \tag{22}$$

which can be written as

$$\alpha_{n+1}=f(\alpha_n,M).$$

Since a, a_1, b_1 are not functions of M, if we replace M with $1/M$ in Eq. (22), we get back the same equation. This shows that

$$f(\alpha_n,M)=f(\alpha_n,1/M). \tag{23}$$

It should be noted that the map is invariant only when there are no sudden lift-offs between two iterates of the map. This is true for an interval close to the fixed point on the right. However, the entire map between two adjacent fixed points is not invariant under $M\rightarrow 1/M$.

Observation. The minimum value of the interval of attraction for each fixed point occurs at $M=1$.

Although it is difficult to prove analytically that the minimum occurs at $M=1$ for the exact map, all numerical results suggest exactly that. From the approximate map, Eq. (19), and the subsequent estimate of the basin of attraction, $\Delta=\lambda^{-3}$, it is easy to prove that the minimum size of the basin of attraction occurs at $M=1$. The invariance of the map

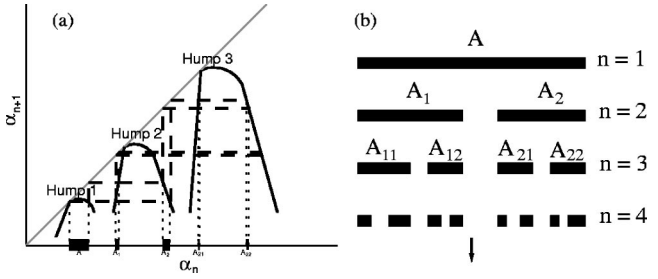

FIG. 5. (a) A schematic map showing the local basin of attraction A of the first fixed point, its preimages A_1 and A_2, and their preimages A_{21} and A_{22}, etc. (b) Construction of the basin of attraction of α^{*1} leads to a Cantor set. The basin of attraction contains all segments including the Cantor set.

under the inversion of M makes $M=1$ to be an extremum point. We claim that this point corresponds to the minimum size of the basin of attraction on the basis of numerical results.

V. GLOBAL MAP AND THE EFFECT OF SYSTEM PARAMETERS

The mass ratio M is the only nondimensional parameter apart from α which affects the dynamics. Figure 2 shows how the map varies with M between two successive fixed points. For low values of M, the entire map is above the line $\alpha_{n+1}=\alpha^{*1}$. Hence, the entire interval becomes an interval of attraction. As M is increased, increasingly larger portions of the map drop below the line $\alpha_{n+1}=\alpha^{*1}$. Consequently, the interval of attraction shrinks till $M=1$ where it is minimum. As M is increased further, the interval of attraction also increases. This feature leads to a complex basin of attraction as we show in Sec. VI.

VI. GLOBAL BASIN OF ATTRACTION

The local basin of attraction of a fixed point of the map is discussed in Sec. IV A. We now try to answer the following question. Are there other initial conditions apart from the ones in the local interval of attraction around a fixed point that lead to incessant hopping? That is, we seek other initial conditions, say $\hat{\alpha}$, such that $f^n(\hat{\alpha})\rightarrow\alpha^*$ as $n\rightarrow\infty$. For any given M, this basin of attraction is naturally limited to 1D [14]. We, however, consider the variation in the mass ratio as well and construct the global basin of attraction in the M-α plane.

A. Construction of the basin of attraction

For a constant M, it turns out that there are infinite number of intervals of initial conditions that are in the α-limit set of a given fixed point. To illustrate this, we use a schematic drawing of the multimodal map and construct the global basin of attraction of the first fixed point. The schematic map shown in Fig. 5(a) captures the essential geometric features of the original map.

Let us consider the first fixed point α^{*1}. Let us denote the local basin of attraction of α^{*1} by A and let S be its global basin of attraction, i.e., $S=\{\alpha|f^n(\alpha)\rightarrow\alpha^{*1}$ as $n\rightarrow\infty\}$. Naturally, $A\subset S$. Now, we consider the preimage of A. From the geometric construction shown in Fig. 5(a), we see that two distinct intervals A_1 and A_2 from the next hump map into A. That is,

$$f^{-1}(A)=A_1\cup A_2\Rightarrow(A_1\cup A_2)\subset S.$$

We can iterate backwards again and find the preimages of A_1 and A_2:

$$f^{-1}(A_1)=A_{11}\cup A_{12}\Rightarrow(A_{11}\cup A_{12})\subset S.$$

Continuing, thus, with the preimages, we get

$$\cup A_{ijkl\ldots}\subset S.$$

Thus, the global basin of attraction S is made up of all these segments that, in the limit, form a Cantor set. The formation of the Cantor set is rather obvious from Fig. 5(b). However, we must point out that although S contains a Cantor set, its topology is not equivalent to that of a Cantor set since it contains all the previous pieces of the Cantor set construction which have finite measure. Since the topological character of the map is the same for all fixed points, the structure of S remains the same for all fixed points.

B. Nested basins of attraction

We have infinite number of fixed points and every fixed point has its own basin of attraction, entirely disconnected from the basins of attraction of other fixed points. Each basin of attraction has a complex topology since it contains sets of finite as well as zero measure (with infinite number of elements). The global basin of attraction of lossless motions consists of the global basin of attraction of each fixed point. Thus, we get an intricately woven, or rather nested, basin of attraction. This intricate nesting becomes more and more pronounced as we explore higher values of α.

The numerically generated basin of attraction is shown in Figs. 6–9. We follow a color scheme (shown as shades of gray in the printed figures). We plot all points which lead to the first fixed point $\alpha^{*1}=4.493$ with green, the points which lead to the second fixed point $\alpha^{*2}=7.7252$ with red, the points leading to the third fixed point with blue, and so on (Fig. 6).

The figure shows that at lower values of M, the global basin of attraction is fairly large. In fact, for $M=0.1$, the entire range of α shown in Fig. 6 looks green, i.e., most points seem to belong to the basin of attraction of α^{*1}. To validate this, we took $\alpha^{*1}\leqslant\alpha\leqslant\alpha^{*6}$, subdivided the range into five intervals (going from α^{*i} to α^{*i+1}), took 10 000 equally spaced points in each interval and tracked the fate of their orbits. We calculated the fraction of the number of initial conditions from each interval that eventually ended up in the basin of attraction of one or the other fixed point. We then added up the fractions from each interval to estimate the measure of the basin of attraction of each fixed point as well as all of them together within, of course, the finite range of α. For $M=0.1$, we found the measure of the ''global'' basin

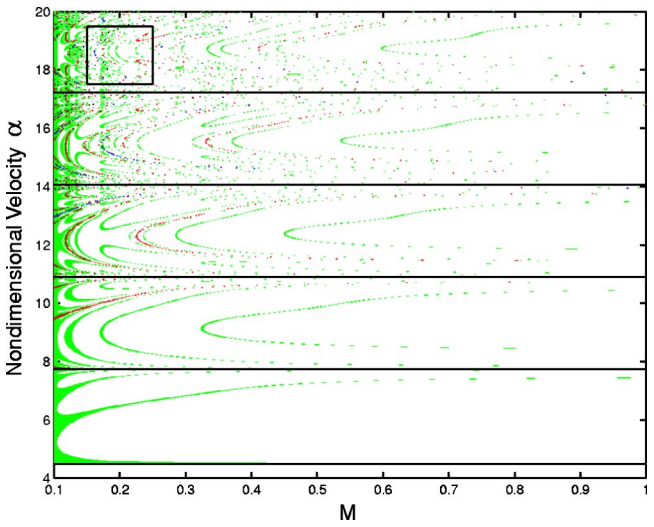

FIG. 6. The basin of attraction for the hopping model for small M. The initial conditions whose iterates converge to a particular fixed point are shown by a particular shade of gray or color. The inset is shown in detail in Fig. 8.

(up to α^{*6}) of attraction of incessant motions to be 1 Thus, all initial conditions within the selected range ended up in the basin of attraction of one or the other fixed point. A majority of these points, however, get attracted to the first fixed point whose basin of attraction measures 0.953. This is why most points in Fig. 6 look green at $M=0.1$. However, for $M=0.2$, the same measure (for all fixed points together) turns out to be 0.037, i.e., only 3.7% of the initial conditions lead to lossless motions. As Fig. 6 shows, this measure of the initial conditions that belong to the global basin of attraction of the incessant motions decreases rapidly as M increases and then starts increasing again as M becomes very large.

It is evident from the basins of attraction that this simple system exhibits complex dynamics. Although the basin of attraction of any one fixed point is filled with holes that

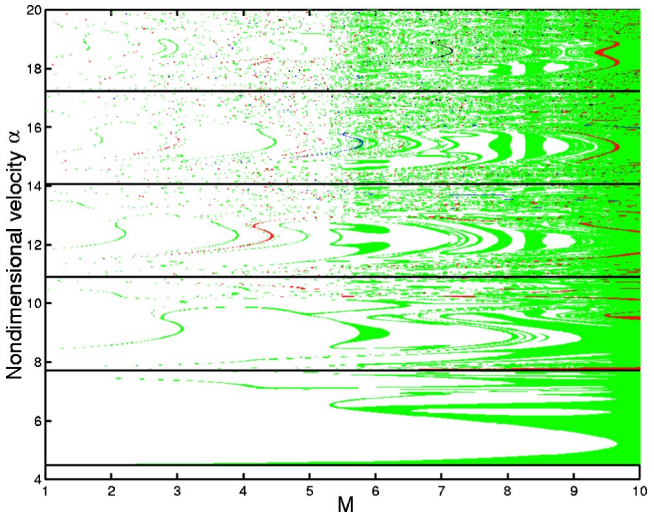

FIG. 7. The basin of attraction for the hopping model for $M=1-10$. The structure in the basin for large M (close to $M=10$) contains similar structure as that for small M (see Fig. 6).

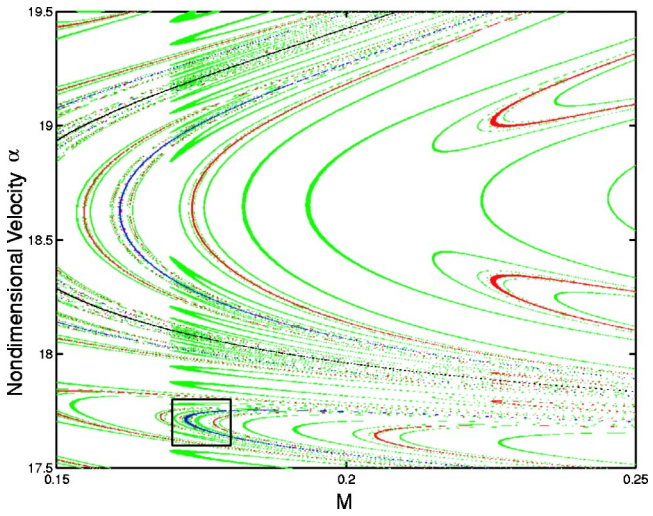

FIG. 8. The inset of Fig. 6 is shown in greater detail here revealing the structure of the basin. The structure at finer scales is evident in the figure.

belong to the basin of attraction of other fixed points and hence seems *riddled* [15], it remains to be proved if these are indeed riddled basins [16]. Although it is difficult to predict the fate of an arbitrary initial condition, especially for very large α, because in the neighborhood of every initial condition which would settle down to a particular fixed point, there exists another initial condition which would settle down to some other fixed point or may not settle down to any fixed point at all, the degree of unpredictability in the *qualitative* dynamics of the systems is not as pronounced as in the system described by Sommerer and Ott [15]. It is debatable whether two extremely close initial conditions leading to two different fixed points in this case qualify to be called seeds of qualitatively different dynamics. From a practical point of view, both such motions are lossless incessant motions of the hopper. However, they have considerably different energies and their mid-air dynamics are certainly quite different. Apart from such motions, any initial condition (for

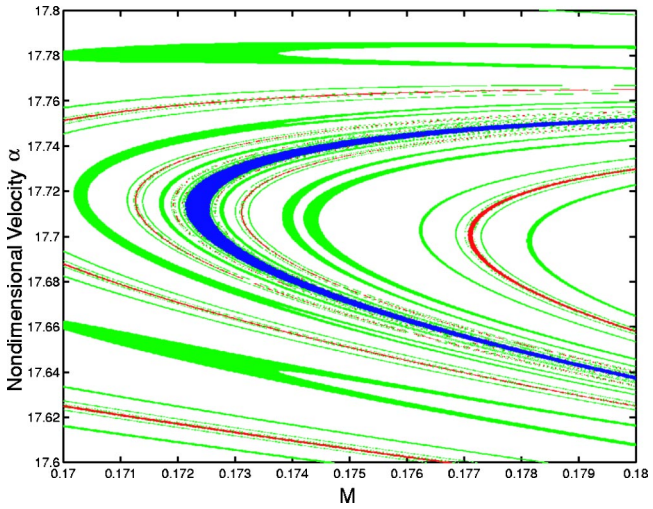

FIG. 9. The inset of Fig. 8 is shown here revealing the structure of the basin at a further finer scale.

large α) contains points in its neighborhood which lead to no hops at all or a few initial hops and then no hops.

VII. CONCLUSIONS AND REMARKS

We have studied the global dynamics of a passive hopper, modeled by two masses connected with a single spring. The basic dynamics of the model, including the existence of incessant motions, has been reported previously [1]. Here, we have studied the multimodal map associated with the dynamics of the hopper in greater detail. The map variable α, the nondimensional velocity of the upper mass, completely characterizes the energy of the system at gradual takeoffs. There is only one system parameter—the mass ratio M. We use the one-dimensional map to first describe the dynamics of the hopper in different regions of the map for a given value of M and then show how the dynamics changes when we vary M. In particular, we show that the map close to the fixed points is invariant under the inversion of M, i.e., $M \rightarrow 1/M$.

Next, we show that the fixed points exhibit one-way stability by constructing and analyzing an approximate analytical map. We use the approximate map to estimate the size of the local basin of attraction. We also show that the size of the local basin depends upon the system parameter M. We then construct the global basin of attraction, the set of all initial conditions, for different values of the mass ratio M, that settle down to a fixed point. This basin of attraction is complex and shows structure at finer scales. The complex structure of the basin contains regions with interwoven Cantor-like sets that render predicting the final state of an initial condition difficult. We have also estimated the measure of the basin of attraction over a finite range of α for a given M.

ACKNOWLEDGMENTS

This work was supported by the Department of Science and Technology under the Robotics and Manufacturing PAC and by NSG funding. The authors wish to thank Professor Anindya Chatterjee for his suggestion on computing the measure of the basins, and Professor Andy Ruina for his critical comments on the paper and for bringing Hagerty's work to our attention.

[1] A. Chatterjee, R. Pratap, C.K. Reddy, and A. Ruina, Int. J. Robot. Res. **21**, 621 (2002).
[2] T. McGeer, Int. J. Robot. Res. **9**, 62 (1990).
[3] M. Garcia, A. Chatterjee, and A. Ruina, Dyn. Stab. Syst. **15**, 75 (2000).
[4] M. Garcia, A. Chatterjee, and A. Ruina, ASME J. Biomech. Eng. **120**, 281 (1998).
[5] W. Schiehlen and J. Gao, Z. Angew. Math. Mech. **69**, 302 (1989).
[6] P. J. Hagerty Ph.D. thesis, University of Michigan, 2001.
[7] R.M. May, Nature (London) **261**, 459 (1976).
[8] A. Ruina and J. Bertram (unpublished).
[9] R. Devaney, *An Introduction to Chaotic Dynamical Systems* (Addison-Wesley, New York, 1987).
[10] R. Pratap, S. Mukherjee, and F.C. Moon, Phys. Lett. A **170**, 384 (1992).
[11] A.S. Matveev, and A. Savkin *Qualitative Theory of Hybrid Dynamical Systems* (Birkhauser Boston, Cambridge, MA, 1999).
[12] B.F. Feeny and F.C. Moon, Nonlinear Dyn. **4**, 25 (1993).
[13] S.W. Shaw and P.J. Holmes, J. Sound Vib. **90**, 129 (1983).
[14] C.K. Reddy, and R. Pratap Current Science **79**, 639 (2000).
[15] J.C. Sommerer and E. Ott, Nature (London) **365**, 138 (1993).
[16] J.A. Alexander, J.A. Yorke, Z.-P. You, and I. Kan, Int. J. Bifurcation Chaos Appl. Sci. Eng. **2**, 795 (1992)